JTTEE5 5:431-438

Influence of Dopant on the Thermal Properties of Two Plasma-Sprayed Zirconia Coatings Part I: Relationship between Powder Characteristics and Coating Properties

R. Hamacha, P. Fauchais, and F. Nardou

Plasma-sprayed coatings produced with two zirconia powders (-90 + 10 μm, spray dried and partially sintered) that were stabilized (9 wt%) with dysprosia (DSZ) and ytterbia (YbSZ) were compared to coatings sprayed with a yttria (7 wt%) stabilized zirconia (YSZ) powder (45 + 22 μm, fused and crushed). The YSZ particles in the coating were almost fully molten (less than 0.2% monoclinic m-phase), with excellent contact between the layered splats (adhesion of 54 MPa). The DSZ particles were only partially melted (3.1% m-phase), with coating adhesion greater than 34 MPa; the YbSZ particles were less melted (6.1% m-phase), with coating adhesion of 27 MPa. The thermal properties (diffusivity, a; specific heat, c_p; and thermal conductivity, κ) of the coatings were about the same. Under thermal cycling (1 h heating at 1100 °C in a furnace followed by fast cooling for approximately 3 min by air jets) of the coatings sprayed on FeCrAl alloy manufactured by powder metallurgy, the behavior of the DSZ coating was similar to that of the YSZ, whereas the YbSZ coating was partially detached. However, in all cases the percentage of the monoclinic phase decreased and the ratio of the hexagonal structure increased to 1.013 of the nontransformable tetragonal phase t'.

Keywords dysprosia, partially stabilized zirconia, phase structure, thermal cycling, ytterbia

1. Introduction

PLASMA spraying is widely used to manufacture oxide ceramic coatings on metal components operating at high temperatures in oxidizing atmospheres. Among these ceramic coatings, thermal barrier coatings (TBCs) with a stabilized or partially stabilized zirconia top layer are used to increase the lifetime of components (e.g., piston heads and valves of internal combustion engines, vanes and combustion chambers of aeroengines and gas turbines, heat exchangers, etc.) and/or the operating temperature (Ref 1-4). The role of the TBC is to decrease the component temperature (by about 50 to 100 K) due to the low thermal conductivity (below ~2.5 W/m·K) of the zirconia top layer (generally 0.3 to 0.4 mm thick).

Among the various possible stabilizers (besides MgO and CaO, for $T < 900$ °C), CeO_2 and Y_2O_3 are particularly effective and widely used for $T > 1000$ °C (Ref 1-6). In aeroengines (Ref 7, 8), ZrO_2 + 7 to 8 wt% Y_2O_3 (YSZ) is mostly used. The use of CeO_2 stabilizer is not as popular as that of Y_2O_3 because similar results were obtained on thermal cycling, but with 24 wt% of rare earth oxide stabilizer against 7 to 8 wt%. However, according to the work of Traverse and Foex (Ref 9), other stabilizers can be used. The aim of this paper is to compare the coatings obtained with the fused and crushed YSZ powder to those obtained with two agglomerated powders prepared by H.C. Stark (in the framework of the EU program COST 501). The two powder mixes used were ZrO_2 + 9 wt% Dy_2O_3 (DSZ) and ZrO_2 + 9 wt% Yb_2O_3 (YbSZ). The present work describes the plasma spray arrangement, the sprayed powders and their behavior in the plasma jet, and the coating thermomechanical properties and behavior during thermal cycling.

R. Hamacha, P. Fauchais, and **F. Nardou,** LMCTS-URA CNRS 320, 123 Avenue Albert Thomas, 87060 Limoges Cedex, France, Fax: 55.45.75.86.

2. Setups

2.1 *Plasma Spraying*

Coatings were sprayed on disk-shaped samples (20 mm diam, 4.5 mm thick) made of Fe-22Cr-5.68Al (Kanthal PM alloy obtained by powder metallurgy). The substrates for adhesion tests were FT 25 cast iron, the expansion coefficient of which is very close to that of PM alloy. The substrates were placed on a 110 mm diam cylindrical holder with the rotation axis orthogonal to that of the torch. The torch was moved at a constant velocity (24 mm/s) parallel to the substrate holder axis. The rotation velocity of the substrate holder was adjusted such that overlap of the sprayed beads was 50%—the value corresponding to the best thermomechanical properties of the coatings (Ref 10). Figure 1 shows the experimental setup. Prior to spraying, the substrates were preheated with the plasma jet, and their final surface temperature was controlled by blowing an air jet at the side opposite the plasma torch. This cooling was achieved with a 28 by 1 mm^2 slot placed 5 mm in front of the substrate holder, through which compressed air was passed at up to 1.3 MPa.

The surface temperature of the substrate was measured by an infrared (IR) monochromatic pyrometer (IRCON, 5.2 μm, 10 Hz). Preheating (to about 700 K) was achieved by spraying the Ar-H_2 plasma jet in less than 90 s in order to limit substrate oxidation. A few seconds after powder injection, with a powder flow rate of 1 kg/h, the surface temperature of the coating reached about 750 K. Such a preheating temperature was chosen

to improve the contacts between the splats (Ref 11) and the coating thermomechanical properties (Ref 11, 12). In order to achieve good melting of the relatively large particles of DSZ and YbSZ (–90 + 10 μm), the spraying conditions summarized in Table 1 were chosen. The size distribution of the YSZ powder was smaller (–45 + 22 μm).

Prior to spraying, the substrates were grit blasted with white alumina (mean diameter of 1.4 mm). A pressure blasting machine was used with an 8 mm diam B_4C nozzle orthogonal to the substrates with a compressed air pressure of 0.3 MPa. The blasting distance was 100 mm and the blasting time about 3 s for each substrate; such conditions resulted in an R_a of 13 to 15 μm.

2.2 *Coating and Powder Analysis*

The phase content of powders and coatings was analyzed by X-ray diffraction (XRD). Powder surface and cross-section morphology were observed by using a scanning electron microscope (SEM) equipped with an energy-dispersive spectrometer (EDS). This device was also used to examine polished surfaces and cross sections of the resulting coatings. The coating hardness (12 measurements) was measured on polished coating cross-sections by applying a load of 5 N for 10 s. The coating adhesion/cohesion was measured using the DIN 50160 test; five measurements were carried out for each spraying condition. The specific heat was measured with an isoperibolic calorimeter (Ref 13) and the thermal diffusivity with laser-flash equipment (Ref 14). A furnace with computerized automation allowed the thermal cycling tests to be performed. The samples were treated at 1100 °C for 1 h and, after their withdrawal from the furnace, cooled to room temperature by air jets blown for 3 min. The total cycle, including introduction into and withdrawal from the furnace, lasted 70 min.

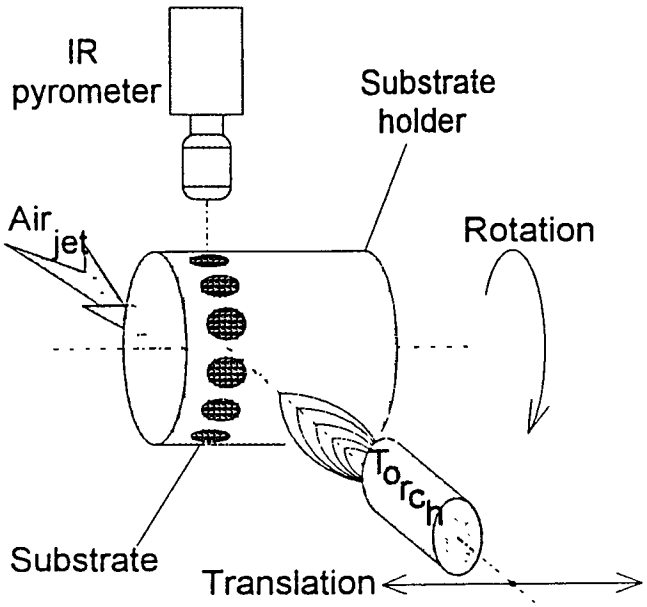

Fig. 1 Spraying device

3. Powder Treatment

3.1 *Feedstock Constituents*

The powders, supplied by H.C. Stark, had a size distribution of –90 + 10 μm and were prepared by agglomeration followed by sintering. Their chemical analysis, provided by the manufacturer, is given in Table 2.

As shown previously (Ref 15, 16), the powder morphology significantly influences the coating thermomechanical properties. This is especially true for zirconia, which, having a low thermal conductivity compared to the mean integrated thermal conductivity of the Ar-H_2 25 vol% plasma gas, promotes the "heat propagation phenomenon" within the particle. Thus, the mean integrated thermal conductivity, $\bar{\kappa}$, is defined by:

$$\bar{\kappa} = \frac{1}{T_p - T_s} \int_{T_s}^{T_p} \kappa(T) \cdot dT$$

where T_p and T_s are, respectively, the plasma and particle surface temperatures, and κ is the thermal conductivity. For Ar-H_2 plasma, κ is drastically enhanced for $T > 4000$ K (i.e., after H_2 dissociation). This propagation phenomenon is enhanced for

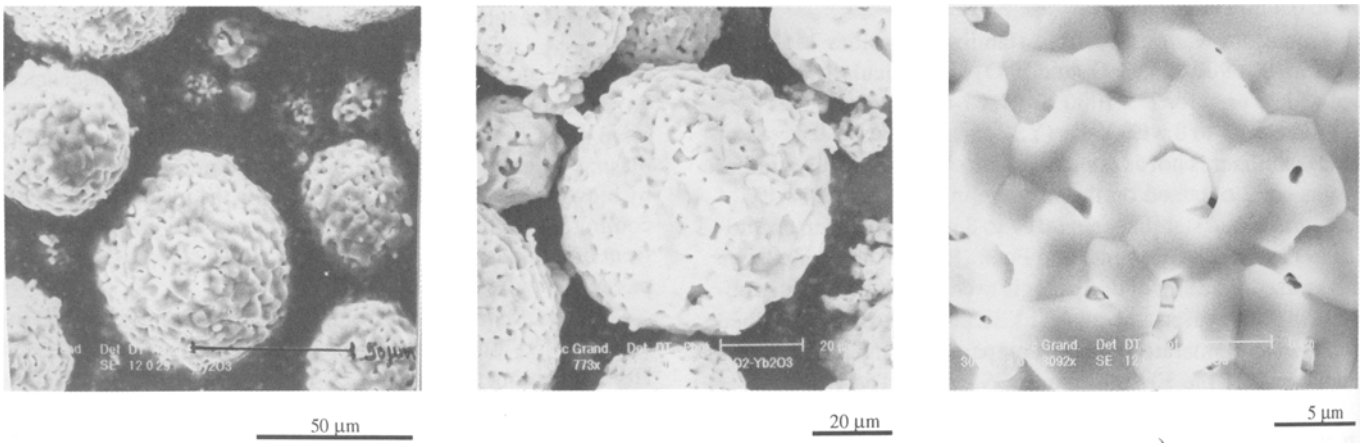

Fig. 2 SEM micrographs of as-received powder morphology. (a) DSZ. (b) YbSZ. (c) Detail of (b)

porous particles formed by agglomeration or agglomeration followed by sintering. The heat transfer within particles in flight in Ar-H_2 dc plasma jets has been examined by Vardelle et al. (Ref 17). Their results have shown that zirconia particles greater than 35 to 40 μm in diameter have a surface temperature that is only slightly greater than their melting temperature. Therefore, the molten shell at the surface of the particles, due to its high viscosity, is blown away by the expansion of gas trapped within the pores. The shell is then no longer in contact with the central part of the particle, which remains unmolten.

As shown in Fig. 2(a) and (b), these two powders consist of agglomerated grains (close to a spherical shape), each a few micrometers in diameter. An enlarged view of the surface of an agglomerated particle (Fig. 2c) shows grain coalescence and the establishment of bridges between them that results from thermal processing of at least 1350 °C after the spray drying procedure. This temperature is greater than or equal to that at which sintering starts, and the observed strong bridging is due not only to the classical growth process in ceramics (superficial diffusion, evaporation-condensation, gaseous diffusion [Ref 18]) but also to volume diffusion (through crystalline cells and/or grain boundaries). A small difference in physical properties exists between both powders (Table 3). For the same monoclinic and tetragonal phase contents, the crystallite size of the YbSZ powder is slightly higher. This might be due to the different action of the dopants, ytterbia probably increasing the diffusion phenomenon and promoting the crystallite size increase. The high percentage of tetragonal phase compared to that of monoclinic phase indicates that the sintering treatment must have lasted several hours.

Mercury porosimetry measurements (Fig. 3) confirmed that the particles are porous. A pore radius greater than 1 μm corresponds to the porosity of the powder bed—that is, the porosity between the particles. To compare the corresponding coatings with those obtained with YSZ, a fused and crushed powder (–45

Table 1 Spraying parameters

Parameter	Value
Plasma torch	
Nozzle id, mm	7
Arc current, A	600
Voltage, V	69
Thermal efficiency, %	59
Gas flow rate, slm	
Argon	45
H_2	15
Powder	
Powder mass flow rate, $\times 10^{-4}$ kg/s	
YSZ	2.25
DSZ	2.33
YbSZ	2.17
Argon carrier gas flow rate, slm	
YSZ	5.5
DSZ	3.2
YbSZ	3.2
Spraying conditions	
Standoff distance, mm	100
Torch translation velocity, mm/s	24
Sample holder rotation, rev/min	180
Substrate roughness (R_a), μm	14 ± 3

Table 2 Chemical composition of the DSZ and YbSZ powders

	Composition							
Powder	HfO_2	SiO_2	Al_2O_3	CaO	Fe_2O_3	MgO	ThO_2	U_3O_8
DSZ	1.75 wt%	0.20 wt%	529 ppm	182 ppm	272 ppm	17 ppm	182 ppm	307 ppm
YbSZ	1.76 wt%	0.17 wt%	453 ppm	378 ppm	329 ppm	17 ppm	171 ppm	330 ppm

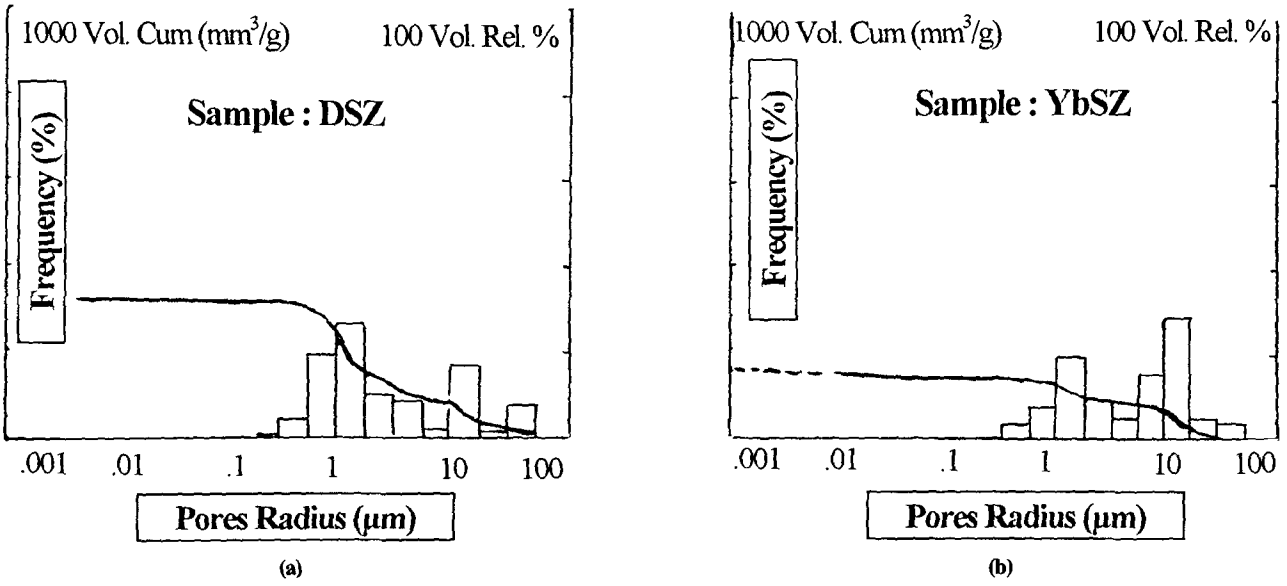

Fig. 3 Mercury porosimetry of DSZ and YbSZ powders

+ 22 μm), Amperit 825-1, was sprayed. This size range was chosen in order to have well-molten particles in the plasma jet according to the spraying conditions summarized in Table 1. As shown by mercury porosimetry, the YSZ powder exhibits pores greater than 1 μm.

It was not possible to achieve better spraying conditions to melt the DSZ and YbSZ particles completely. For arc currents higher than 600 A, due to increased air pumping from the local torch environment, the length of the plasma jet no longer increases (Ref 19) and its temperature distribution does not change; its velocity, however, increases (Ref 20), thus reducing the residence time of the particles.

Table 4 shows the powder densities that were determined. It can be seen that the experimental values correspond well with those calculated by the theoretical law of mixtures. They increase with the atomic mass of the stabilizer. The difference between the theoretical and experimental densities might be due to incorporation of dopant in the zirconia system during the sintering process.

Table 3 Phase contents and crystallite size of the starting powders

Powder type	Phase contents, mol % Monoclinic	Tetragonal	Cubic	Crystallite size [(111)t'], nm
DSZ	12	88	0	51.4
YbSZ	12	88	0	59.1
YSZ	6	94 (t + c)	0	...

Table 4 Powder density determined by helium picnometry

Powder	Density, kg/m^3 Theoretical	Experimental	Plasma sprayed
YSZ	5960	5998	5590(a)
DSZ	6174	6203	5089
YbSZ	6245	6336	5317

(a) Determined by water picrometry

3.2 *Powders after Treatment in the Plasma Jet*

The spraying conditions summarized in Table 1 correspond to well-molten YSZ particles collected in water. More than 95 wt% of powders collected in water have a spherical shape when the starting particles have angular shapes.

The good melting of the fully dense and small particles is confirmed by the lower density of the collected powders (see Table 4). As detailed by Gitzhofer et al. (Ref 21), the solidification of the particles from their surfaces induces internal pores due to the central liquid phase contraction. However, other studies on porous YSZ particles (-90 + 45 μm) (Ref 15) show that the melting behavior of the porous DSZ and YbSZ particles (whose mean diameter is about 70 μm) is inferior to that of smaller YSZ particles. This is illustrated in Fig. 4, where broken particles exhibit porous structures.

The cross sections of the powders agree with the calculations of Vardelle et al. (Ref 17) as well as the results on porous YSZ (Ref 15). Many particles, especially those greater than 40 μm diam, are spheres with a well-molten crust and an unmolten core. This is seen in Fig. 5 in relation to plasma-treated YbSZ particle cross sections. This powder exhibits more porous particles than DSZ, even though the porosity of the starting powder is lower (see Fig. 3) and the porosity variation after plasma treatment (see Table 4) is only 16% for this powder compared with 18% for the DSZ powder. This might correspond to the existence of more molten impervious shells. It is also interesting that

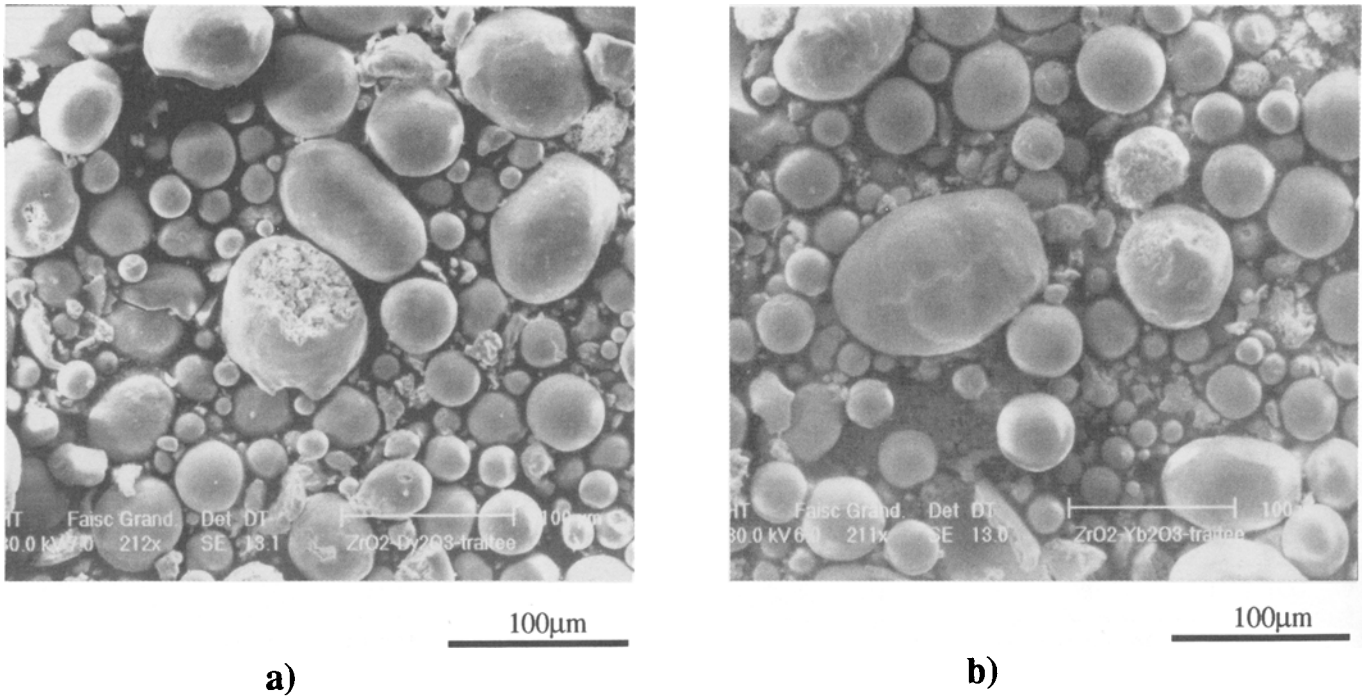

Fig. 4 SEM micrographs of powder surface morphology after passage in the plasma jet. (a) DSZ. (b) YbSZ

the highest weight percentage of Yb_2O_3 is in the central untreated core of the particle (Fig. 5b).

4. Coatings

4.1 *Structure and Phase Composition*

The coatings, analyzed by XRD, contain mainly the metastable tetragonal phase t', with a small amount of monoclinic m-phase. When completely molten particles impact on the substrate, the resulting splats cool at velocities of up to 5.10^8 K/s just after or even during flattening and at greater than 10^6 K/s when solidification has started (Ref 11). Such high cooling rates explain the formation of t'-phase. For partially molten particles, the m-phase is retained (Table 5). These results confirm the good melting of the YSZ powder (no remaining monoclinic phase when compared with the starting powder in Table 3) and the better melting of the DSZ powder compared with YbSZ. The dopant evaporation that was seen for the YbSZ particles (Fig. 5b) may also participate in the retention of m-phase. The cross sections of the coatings revealed the presence of unmolten particles, especially in the YbSZ coatings compared with the DSZ coatings.

Scanning electron micrographs of the coatings after fracture reveal a typical lamellar structure in all three coatings. However, compared to the DSZ coating (Fig. 6), the YbSZ coating (Fig. 7) exhibits poor contact between the successive passes. Each pass represents about four to five piled splats, each between 1.5 and 2 μm thick. When the surface temperature of the substrate (Ref 22) or the previously deposited layer (Ref 23) is higher than 200 °C, the thermal contact resistance between the splat and the layer underneath is lower than 10^{-7} K · m^2/W. Therefore, the cooling of the splat, just after flattening, is very fast (>10^7 K/s), resulting in a columnar structure within the splat (Ref 24) (for both coatings in Fig. 6 and 7). When the surface temperature of the splat upon impact of the next splat is higher than 2000 K (temperature determined by the calculations of Vardelle et al. [Ref 17]), the columnar growth of the new impacting splat extends the columns of the already solidified one. Thus, within one pass it is possible to achieve a columnar growth within the piled splats from the bottom to the top of the pass (Ref 25). The mode of fracture between the successive passes may be due either to an insufficient surface temperature to achieve a columnar growth between two successive passes and/or to residual stresses generated upon cooling between the successive passes. It might also be connected to the presence of a vitreous phase between the columnar grains (Ref 7), probably generated by impurities in the powders, especially SiO_2 (Ref 26).

4.2 *Thermomechanical Properties*

The values summarized in Table 6 agree with our remarks about particle melting. Therefore, (1) the adhesion, related to the contact between the piled splats and the successive passes, is

Table 5 Molar phase composition of the coatings

Powder	Monoclinic phase, mol %
YSZ	0 ± 0.1
DSZ	3.3 ± 0.1
YbSZ	6.1 ± 0.1

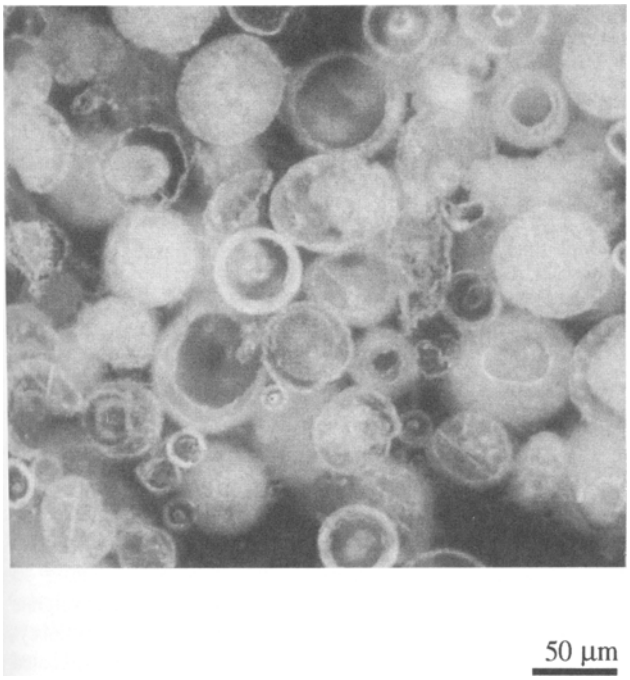

a)

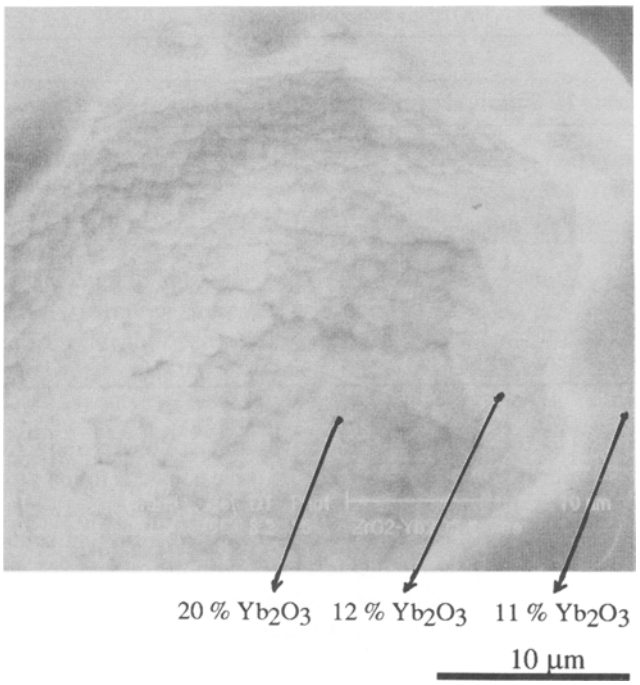

b)

Fig. 5 SEM-EDS micrographs of YbSZ particle cross sections after passage in the plasma jet

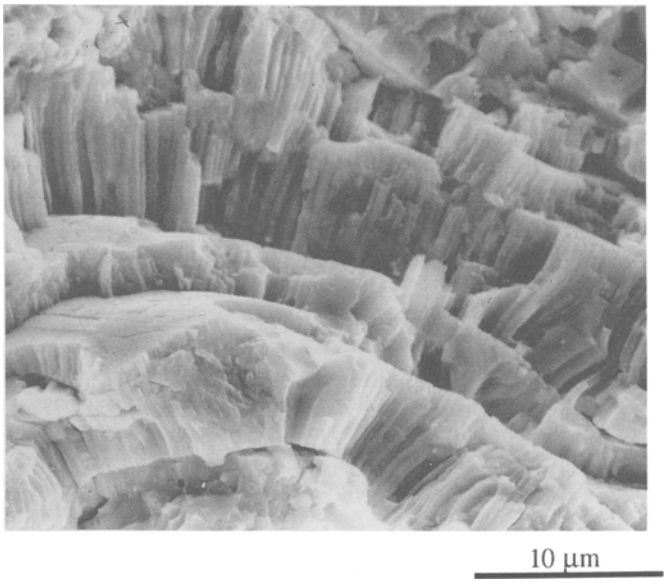

Fig. 6 SEM micrograph of fractured surface of DSZ coating

Table 6 Mechanical properties of the coatings

Powder	Adhesion, MPa	Hardness, HV_5 As sprayed	Hardness, HV_5 After n cycles	Coating surface roughness (R_a), μm
YSZ	58 ± 6	791 ± 46	843 ± 43 (n = 400)	5.2 ± 0.1
DSZ	>35(a)	695 ± 32	887 ± 25 (n = 600)	10 ± 1
YbSZ	27 ± 5	632 ± 36	961 ± 134 (n = 478)	12 ± 2

(a) For three samples, rupture occurred in the glue.

Table 7 Thermal properties of the coatings at 600 °C

Powder	Diffusivity (a), 10^{-7} m^2/s	Specific heat (c_p), 10^3 J/kg · K	Density (ρ), kg/m^3	Calculated thermal conductivity (κ)(a), W/m · K
YSZ	1.8	0.40	5600	4.0
DSZ	1.5	0.38	5800	3.3
YbSZ	1.4	0.5	5400	3.8

(a) $\kappa = a \cdot c_p \cdot \rho$

highest for the YSZ coating and lowest for the YbSZ coating; (2) the hardness, which also depends on these contacts, follows the same trend; (3) the small, well-molten YSZ particles cover the irregularities of the layers already deposited, resulting in the lowest open porosity, which increases with the quantity of unmolten particles; and (4) the substrate surface roughness is low for the well-molten particles (YSZ) and high for the poorly molten particles (YbSZ).

Table 7 summarizes the thermal properties of the coatings. The thermal conductivity (κ) has been calculated from the values of the measured diffusivity (a), specific heat (c_p), and density (ρ). These values were measured between 400 and 1100 °C.

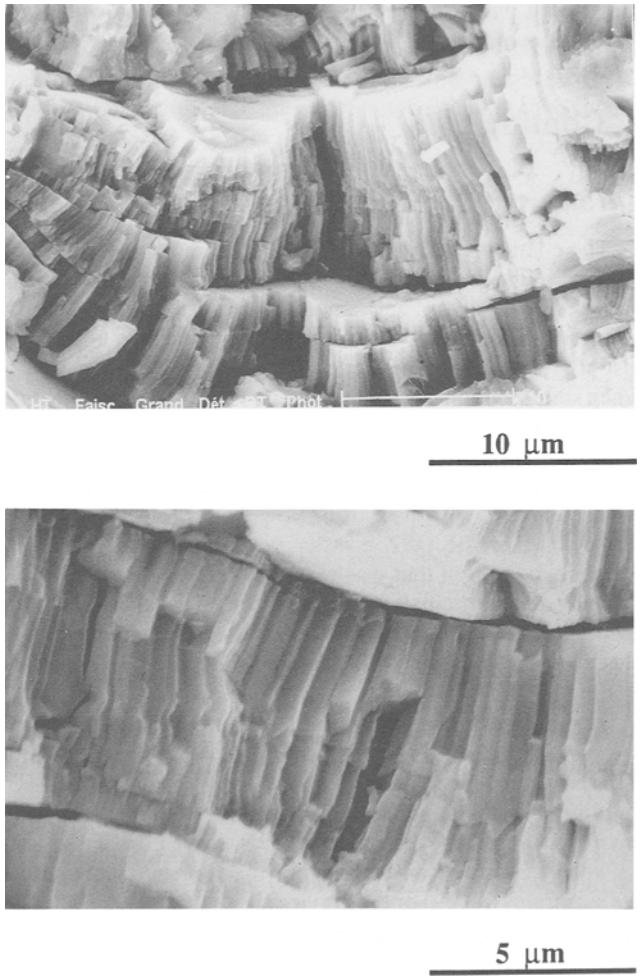

Fig. 7 SEM micrographs of fractured surface of YbSZ coating. (a) Separation between lamellae, denoting a weak interlamellar contact. (b) Detail of (a)

Above 500 °C the parameter a is almost constant and c_p and ρ vary very slightly and almost linearly with temperature (Ref 27, 28). The values given in Table 7 were evaluated at 600 °C. The highest thermal conductivity is obtained with the YSZ powder, for which the contacts between the splats and passes are the best.

4.3 *Coating Behavior under Thermal Cycling*

Tests were performed with the FeCrAl substrate. First, a weight gain of the coating and substrate was noticed. It arose essentially from oxidation of the noncoated part of the ferritic substrate. During the initial cycles, air penetration can occur through pores and microcracks on the ceramic side of the coatings, leading to the formation of an alumina layer at the coating/substrate interface. Moreover, zirconia, being a semiconductor to anionic vacancies, allows oxygen to migrate easily. Most of the mass increase took place during the initial cycles, and the weight gain was practically that of the noncoated substrate. The mass gain of the YbSZ coating was fastest.

Scanning electron micrographs of polished coating cross sections are shown in Fig. 8 for the DSZ and YbSZ coatings. After more than 400 cycles, both coatings present dense and coher-

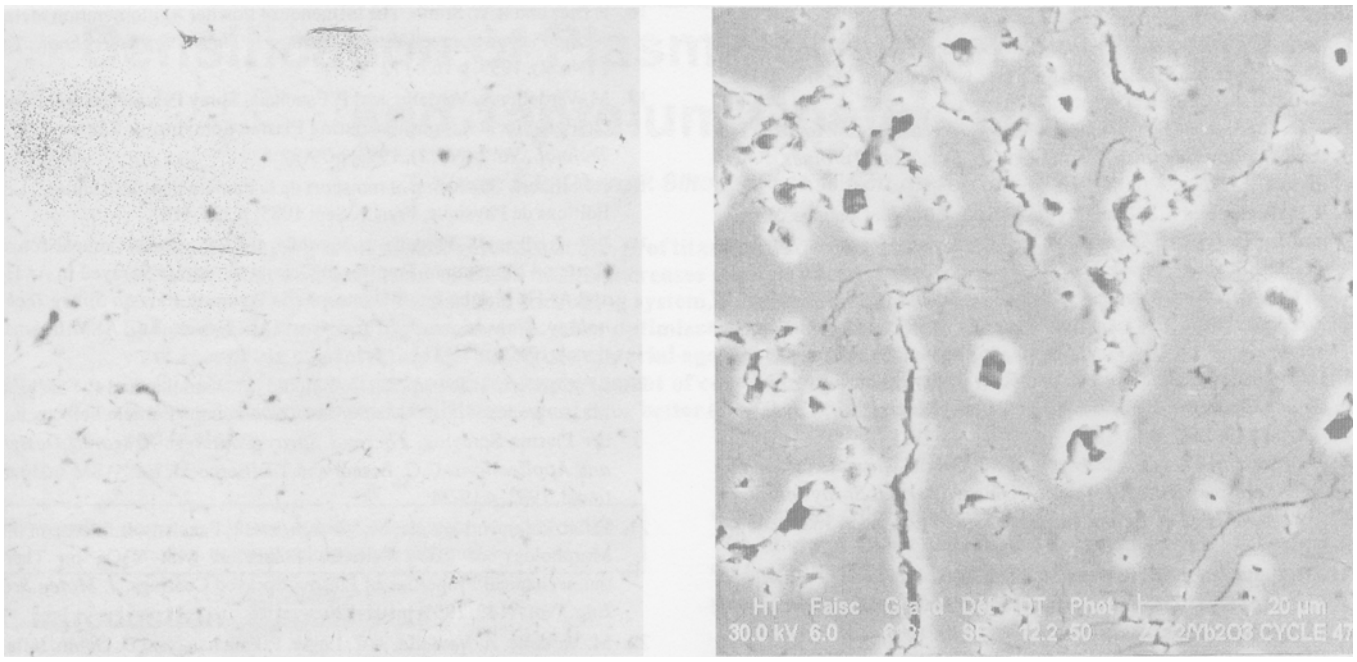

a) b)

Fig. 8 SEM micrographs of cross sections of cycled coatings. (a) YbSZ. (b) DSZ

ent features with a better interlamellar contact for the DSZ material than before thermal cycling. This is probably due to sintering curing of microcracks and the development of interlamellar zones. Such results are confirmed by the hardnesses measurements shown in Table 6. Conversely, the YbSZ coating exhibits a completely different structure with decohesion (Fig. 7a) as well as more cracking closer to the substrate. This is confirmed by the microhardness (Table 6), which is slightly lower for the YbSZ coating.

For the YSZ coating no monoclinic phase is revealed during thermal cycling, whereas for the two other coatings it is reduced: from 3.3 to 1.86% for the DSZ coating after 120 cycles and further to 0 after 600 cycles and from 6.1 to 1.3% for the YbSZ coating after 630 cycles. All coatings show an increase in the *c/a* ratio with thermal cycling (Table 8). This value tends to be 1.013, which is that of the t′-phase.

5. Conclusions

Two powders stabilized with 9 wt% Dy_2O_3 and Yb_2O_3 were tested for a TBC application. They were prepared by spray drying a slurry of small particles (below 2 μm); the spray-dried particles were sintered afterward to at least 1350 °C. The resulting powders were rather porous with a size distribution of –90 + 10 μm. The spraying conditions used with an Ar-H_2 (25 vol%) dc plasma jet were excellent for melting smaller particles (–45 + 22 μm, 7 wt% yttria stabilized, fully dense) but less suitable for large particles. Moreover, porosity resulted in spheres with an unmelted core (especially for particles larger than 40 μm diam).

Table 8 Increase in the *c/a* ratio with thermal cycling

Powder	Increase in *c/a* ratio, %
YSZ	13.5
DSZ	17.3
YbSZ	16.5

The melting problem was more crucial for the Yb_2O_3 particles. The monoclinic phase of the as-sprayed coatings was 0% for YSZ, 3.3% for DSZ, and 6.1% for YbSZ, which agrees well with the melting conditions.

The coating adhesion (on FT 25 cast iron substrates) and Vickers hardness decreased in the order of YSZ, DSZ, and YbSZ, while the open porosity increased. Although differences in the splat contacts, as seen by SEM and adhesion/cohesion measurements, were observed, the thermal properties of the coatings do not appear to be characteristic of the stabilizers. Thermal cycling at 1100 °C, with a fast cooling (3 min) by air jets after 1 h of heating in a furnace, has resulted in excellent resistance of the YSZ and DSZ coatings and poor properties of the YbSZ coating. Thermal cycling (600 cycles) significantly reduces the monoclinic phase to zero for DSZ and 1.3% for YbSZ coatings and increases the *c/a* ratio of the hexagonal structure to the theoretical value of 1.013 of the t′-phase. To achieve a better comparison between new stabilizers and yttria, these measurements should be performed again using –45 + 22 μm powders (presently unavailable). Our results show that the dysprosia-stabilized powder (–90 + 10 μm) behaves as well as the yttria-stabilized material (–45 + 22 μm).

References

1. S. Stecura, "Two Layer Thermal Barrier Coating for Turbine Airfoils—Furnace and Burner Rig Test Results," NASA Tech. Memo. X-3425, NASA-Lewis Research Center, 1976
2. K.D. Sheffler and D.K. Gupta, Current Status and Future Trends in Turbine Applications of T.B. Coatings, *J. Eng. Gas Turbines Power (Trans. ASME)*, Vol 110, 1988, p 605-625
3. R.V. Bratton and K.S. Lau, Zirconia Thermal Barrier Coatings, *Science and Technology of Zirconia*, Vol 3, *Advances in Ceramics*, American Ceramic Society, 1984, p 226-238
4. N. Claussen, M. Ruhle, and A. Hever, in *Science and Technology of Zirconia*, Vol 2, *Advances in Ceramics*, American Ceramic Society, 1984
5. C.C. Chang, W. Phucharoen, and R.A. Miller, Behavior of Thermal Barrier Coatings for Advanced Gas Turbine Blades, *Surf. Coat. Technol.*, Vol 30, 1987, p 13-28
6. Ch. Merterns-Lecomte, D. Mack, and J. Garcia, Characterization of a New Aerospace Thermal Barrier Coating, *Thermal Spray Industrial Applications*, C.C. Berndt and S. Sampath, Ed., ASM International, 1994
7. P.D. Harmsworth and R. Stevens, Phase Composition and Properties of Plasma Sprayed Zirconia Thermal Barrier Coatings, *J. Mater. Sci.*, Vol 27, 1992, p 611-615
8. P.D. Harmsworth and R. Stevens, Microstructure of Zirconia-Yttria Plasma Sprayed Thermal Barrier Coatings, *J. Mater. Sci.*, Vol 27, 1992, p 616-624
9. J.P. Traverse and M. Foex, Zirconia Stabilization, *Rev. Int. Hautes Temp. Réfract.*, Vol 65, 1961, p 2048-2056
10. D. Bernard and P. Fauchais, Influence of the Torch-Substrate Relative Movements and Cooling of the Coatings during Spraying on the Mechanical Properties of TBCs, *Thermal Spray Research and Applications*, T.F. Bernecki, Ed., ASM International, 1991, p 551-560
11. S. Fantassi, M. Vardelle, A. Vardelle, and P. Fauchais, Influence of the Velocity of Plasma Sprayed Particles on Splat Formation, *J. Therm. Spray Technol.*, Vol 2 (No. 4), 1993, p 379-384
12. L. Bianchi, F. Blein, A. Grimaud, and P. Fauchais, Comparison of Plasma Sprayed Alumina and Zirconia Coatings by RF and DC Plasma Spraying, *Thermal Spray Industrial Applications*, C.C. Berndt and S. Sampath, Ed., ASM International, 1994, p 575-581
13. E. Mariage, "Measurement of the Specific Heat of Solids at High Temperatures and of the Heat Flux Imposed to a Wall by a dc Plasma Jet," Ph.D. thesis, University of Limoges, Limoges, France, Dec 1990
14. R. Brandt, L. Pawlowski, G. Neuer, and P. Fauchais, Specific Heat and Thermal Conductivity of Plasma Sprayed Yttria-Stabilized Zirconia and NiAl, NiCr, NiCrAl, NiCrAlY, NiCoCrAlY Coatings, *High Temp.-High Press.*, Vol 19, 1986, p 65-77
15. M. Vardelle, A. Vardelle, A. Denoirjean, and P. Fauchais, Heat Treatment of Zirconia Powders with Different Morphologies under Thermal Plasma Conditions, *MRS Spring Meeting Proc.*, Vol 190, 1991, p 175-183
16. P. Diez and R.W. Smith, The Influence of Powder Agglomeration Methods on Plasma Sprayed Yttria Coatings, *J. Therm. Spray Technol.*, Vol 2 (No. 2), 1993, p 165-172
17. M. Vardelle, A. Vardelle, and P. Fauchais, Spray Parameters and Particle Behavior Relationships during Plasma Spraying, *J. Therm. Spray Technol.*, Vol 2 (No. 1), 1993, p 79-92
18. J. Philibert, "Diffusion et transport de la matière dans les solides," Les Editions de Physique, France, Sept 1985, p 391-410
19. P. Roumilhac, M. Vardelle, A. Vardelle, and P. Fauchais, Comparison of Heat and Momentum Transfer to Ceramic Particles Sprayed in Ar-H_2 and Ar-He Plasma Jets at Atmospheric Pressure, *Plasma Spray Technology: New Ideas and Processes*, D.L. Houck, Ed., ASM International, 1989, p 111-117
20. J.F. Coudert, M.P. Planche, O. Betoule, M. Vardelle, and P. Fauchais, Measurement of Flow Velocity and Correlation to Particle Velocity under Plasma Spraying, *Thermal Spray Coatings: Research Design and Applications*, C.C. Berndt and T.F. Bernecki, Ed., ASM International, 1993, p 19-24
21. F. Gitzhofer, A. Vardelle, M. Vardelle, and P. Fauchais, Influence of the Morphology of ZrO_2 Particles Stabilized with Y_2O_3 on Thermomechanical Properties of Plasma-Sprayed Coatings, *J. Mater. Sci. Eng.*, Vol A147, 1991, p 107-120
22. M. Vardelle, A. Vardelle, A.C. Leger, P. Fauchais, and D. Gobin, Influence of the Particle Parameters at Impact on Splat Formation and Solidification in Plasma Spraying Processes, *J. Therm. Spray Technol.*, Vol 4 (No. 1), 1995, p 50-58
23. P. Fauchais, M. Vardelle, A. Vardelle, L. Bianchi, and A.C. Leger, Parameters Controlling the Generation and Properties of Plasma Sprayed Zirconia Coatings, *Plasma Chem. Plasma Process.*, Vol 16 (No. 1), 1996, p 99S-125S
24. L. Bianchi, P. Lucchese, A. Denoirjean, and P. Fauchais, Microstructural Investigation of Plasma-Sprayed Alumina Splats, *Advances in Thermal Spray Science and Technology*, C.C. Berndt and S. Sampath, Ed., ASM International, 1995, p 255-260
25. A. Haddadi, F. Nardou, A. Grimaud, and P. Fauchais, Generation of the First Layers of Zirconia Plasma Sprayed Coatings: Correlation between Splat Layering and Spraying Parameters, *Advances in Thermal Spray Science and Technology*, C.C. Berndt and S. Sampath, Ed., ASM International, 1995, p 249-254
26. R.A. Miller, W.J. Brindley, J.G. Goedjen, R. Tiwarni, and D. Mess, The Effect of Silica on the Cyclic Life of a Zirconia-Yttria Thermal Barrier Coating, *Thermal Spray Industrial Applications*, C.C. Berndt and S. Sampath, Ed., ASM International, 1994, p 49-55
27. G. Gasgnier, "Yttria Densification," Ph.D. thesis, University of Limoges, Limoges, France, 1991
28. R. Hamacha, "Contribution to the Study of Plasma Sprayed Coatings: Influence of Thermal Post Treatments and Nature of the Zirconia Stabilizer," Ph.D. thesis, University of Limoges, Limoges, France, March 1994